Numerical Analysis of the Heat Transfer Behaviour of Water Based Al_2O_3 and TiO_2 Nanofluids in a Circular Pipe under the Turbulent Flow Condition

Goutam Saha and Manosh C. Paul*

Systems, Power and Energy Research Division, School of Engineering, University of Glasgow, Glasgow G12 8QQ, UK

**Corresponding author.* Tel.: +44(0)141 330 8466; fax: +44(0)141 330 4343.

Email address: Manosh.Paul@glasgow.ac.uk (M.C. Paul)

Abstract:

A numerical investigation has been carried out applying single phase approach on turbulent forced convection flow of water based Al_2O_3 and TiO_2 nanofluids flowing through a horizontal circular pipe under uniform heat flux boundary condition applied to the wall. The effect of volume concentrations, Brownian motion and size diameter of nanoparticles on flow and heat transfer have been examined for Reynolds number, $Re = 10 \times 10^3$ to 100×10^3, Prandtl number, Pr = 7.04 to 20.29, nanoparticle volume concentration, χ = 4% and 6% and nanoparticles size diameter, d_p = 10, 20, 30 and 40 nm respectively. Results reveal that the small size of nanoparticles with their Brownian motion has the highest average shear stress ratio, heat transfer rate and thermal performance factor for χ = 6%. Besides, it is found that the heat transfer rate increases as the particle volume concentration and Reynolds number increase with a decrease of nanoparticles size diameter. Moreover, Al_2O_3 water nanofluid shows a higher heat transfer rate compared to that of TiO_2-water nanofluid. Finally, a conclusion has been drawn from the present analysis that the heat transfer performance is more affected by the size diameter and Brownian motion of nanoparticles than the thermal conductivity of nanofluid. Results of the non-dimensional fully developed velocity and turbulent kinetic energy, frictional factor and average Nusselt number for pure fluid (water) as well as the result of average Nusselt number for Al_2O_3 and TiO_2-water nanofluid have been validated with published experimental results as well as with available correlations where a reasonable good agreement has been achieved.

Key words: Nanofluid, Brownian motion, heat transfer rate, thermal performance factor, single phase model.

1. Introduction

Nanofluids are new kind of heat transfer fluids which are derived by stably suspending nanoparticles in conventional heat transfer fluids usually liquids, and the volumetric fraction of the nanoparticles is usually below 5 to 10%. Various applications of nanofluids are found in cooling electronic components [1], transportation [2], industrial cooling [3], heating buildings and reducing pollution [4], nuclear systems cooling [5], space and defence [6, 7], energy storage [8], solar absorption [9], friction reduction [10], magnetic sealing [11], antibacterial activity [12], nanodrug delivery [13], intensify micro reactors [14], microbial fuel cells [15] and so on. Hence, research is in progress to introduce nanofluids in many thermal applications where the conventional fluids such as Ethylene Glycol, engine oil and water are not capable of improving the rate of heat transfer as expected. For the first time, Choi [16] at Argonne National Laboratory used nanoparticles suspended in a conventional heat transfer fluid known as nanofluid and proposed that the addition of nanometer size particles into the base fluid helps to increase the thermal conductivity and hence enhances the heat transfer rate of nanofluid.

Numerous experimental and numerical investigation have been carried out by researchers on different types of pipes or tubes using nanofluids under turbulent flow regime using nanofluid with single phase approach. Qiang and Yimin [17] investigated experimentally the heat transfer characteristics of nanofluid in a circular tube under both laminar and turbulent flow regime. They have measured the heat transfer coefficient and Darcy friction factor of Cu-water nanofluid and showed that the heat transfer rate increased because of addition of nanoparticles in the base fluid, while the Darcy friction factor remained unchanged for different volume fractions. Mansour *et al.* [18] investigated experimentally the effect of physical properties of nanofluid flowing through a tube under constant and uniform heat flux boundary condition. They have demonstrated that the physical parameters vary considerably with the thermophysical properties of the nanofluid. Xuan and Li [19] investigated experimentally the flow and heat transfer behaviour of Cu-water nanofluid. They mentioned that enhancement of heat transfer rate depends on the increase of thermal conductivity or the random movement of the nanoparticles in nanofluid. They introduced a correlation to evaluate the average heat transfer rate of nanofluid under turbulent flow regime. Kim *et al.* [20], on the other hand, studied experimentally the effect of nanofluid on heat transfer flowing through a circular horizontal tube under both laminar and turbulent flow regime. Their investigation revealed that average heat transfer rate increases to 15% and 20% for Al_2O_3-water nanofluid at 3 vol% under both laminar and turbulent flow condition, respectively.

Fotukian and Esfahany [21] investigated experimentally the turbulent heat transfer of Al_2O_3-water nanofluid in a circular tube. Their results indicated that insertion of small amounts of nanoparticles into the base fluid augmented heat transfer remarkably. Sajadi and Kazemi's [22] experimental results on TiO_2-water nanofluid in a circular pipe also showed the same behaviour. Torii [23] however

observed that the forced convective heat transfer rate increased with the volume fraction of nanoparticle flowing through a straight circular tube under constant heat flux boundary condition. Sundar *et al.* [24] investigated experimentally the convective heat transfer and flow behaviours of Fe_3O_4 nanofluid inside a circular tube. It is found that addition of magnetic nanoparticle in the base fluid enhanced the heat transfer rate significantly compared to the other types of nanofluids.

Maiga *et al.* [25] studied numerically the flow and heat transfer behaviours of Al_2O_3-water nanofluid at various nanoparticle volume concentrations in a circular tube under turbulent flow regime. In this study, $Re = 10^4$ to 5×10^5 and the fluid inlet temperature of 293.15 K are considered. Also effect of nanoparticle volume fraction and Reynolds number are presented and a new correlation is proposed. Their numerical outcomes revealed that the inclusion of nanoparticles into the base fluid enhanced the heat transfer rate with the increase of nanoparticle volume fraction. The similar investigation is carried out by Bianco *et al.* [26] using both single phase and multiphase approaches and it is found that the accuracy of the multi-phase mixture model is better than the single phase model. However, Namburu *et al.* [27] analysed numerically the forced convective flow and heat transfer behaviour EG-water based CuO, Al_2O_3 and SiO_2 nanofluids flowing through a circular tube. It is shown that nanofluids have higher viscosity, thermal conductivity and heat transfer rate compared to the base fluid. On the other hand, Kumar [28] studied numerically the heat transfer behaviour of Al_2O_3-water nanofluid using the single phase approach covering both laminar and turbulent flow regime. It is observed that heat transfer rate significantly enhanced in the turbulent flow regime compared to that in the laminar flow regime.

In a practical situation, almost all of the flows are turbulent, and many of these demonstrate extremely high Reynolds numbers e.g. flow in aircraft wings, cars, ships, submarines, turbine blades and large pipe. In order to develop models for energy efficient applications, it is important to understand the phenomena of high Reynolds number turbulence. Therefore, present investigation, which has a particular focus on the thermal energy application, is carried out to explore the effect of Brownian motion and various sizes of nanoparticles of TiO_2-water and Al_2O_3-water nanofluids under the turbulent flow condition for $Re = 10 \times 10^3$ to 100×10^3. In the present investigation, Prandtl number, *Pr*, ranges from 7.04 to 20.29, the particle volume concentration of 4% and 6% and diameter of the nanoparticles of $10, 20, 30$ and $40\ nm$ are considered. To the best of our knowledge, no investigation is carried out to understand the effect of Brownian motion and size of different nanoparticles of Al_2O_3 and TiO_2-water nanofluids considering the above parameters. Hence, the aim of our study is to examine the effect of nanoparticles volume concentration, diameter size and Brownian motion of the nanoparticles on convective heat transfer for Al_2O_3 and TiO_2-water nanofluids using a single phase model.

2. Mathematical modelling

Two approaches have been used by the researchers to investigate the effect of inclusion of nanoparticles into the base fluid [26, 29, 30]. The first approach is the single phase model in which

both the fluid phase and the particles are in thermal equilibrium and flow with the same local velocity while the second approach is the multi-phase model. In the present analysis, single phase approach and two-dimensional axi-symmetric model are considered to describe the turbulent flow and heat transfer behaviour of nanofluids in a horizontal circular pipe under uniform heat flux boundary condition, whereas a multi-phase model is carried out in Saha and Paul [31]. Computational geometry consists of a pipe with length L of 1.0 m and a circular section with diameter, D_h, of 0.019 m as shown in Figure 1. The flow and thermal fields are supposed to be axisymmetric with respect to the horizontal plane parallel to the *x*-axis.

3. Governing equations

The dimensional steady-state governing equations of fluid flow and heat transfer for the single phase model have been presented and the following assumptions are considered:

i. Fluid flow is incompressible, Newtonian and turbulent,

ii. The Boussinesq approximation is negligible as the pipe is placed horizontally,

iii. Fluid phase and nanoparticles phase are in thermal equilibrium and no-slip between them and they flow with the same local velocity,

iv. Nanoparticles are spherical and uniform in size and shape,

v. Radiation effects and viscous dissipation are negligible.

Under the above assumptions, the dimensional steady state governing equations for the fluid flow and heat transfer for the single phase model can be expressed as [32]:

Continuity equation:

$$\frac{\partial v_x}{\partial x}+\frac{\partial v_r}{\partial r}+\frac{v_r}{r}=0 \tag{1}$$

x-momentum equation:

$$\frac{1}{r}\frac{\partial}{\partial x}(rv_xv_x)+\frac{1}{r}\frac{\partial}{\partial x}(rv_rv_x)=-\frac{1}{\rho}\frac{\partial p}{\partial x}+\frac{\mu}{\rho}\frac{\partial}{\partial x}\left[\left(2\frac{\partial v_x}{\partial x}-\frac{2}{3}(\nabla.\vec{v})\right)\right]+\frac{\mu}{\rho}\frac{\partial}{\partial r}\left[\left(\frac{\partial v_x}{\partial r}+\frac{\partial v_r}{\partial x}\right)\right] \tag{2}$$

r-momentum equation:

$$\frac{1}{r}\frac{\partial}{\partial x}(rv_xv_r)+\frac{1}{r}\frac{\partial}{\partial x}(rv_rv_r)=-\frac{1}{\rho}\frac{\partial p}{\partial r}+\frac{\mu}{\rho}\frac{\partial}{\partial x}\left[\left(\frac{\partial v_r}{\partial x}+\frac{\partial v_x}{\partial r}\right)\right]+\frac{\mu}{\rho}\frac{\partial}{\partial r}\left[\left(2\frac{\partial v_r}{\partial r}-\frac{2}{3}(\nabla.\vec{v})\right)\right]-2\frac{\mu}{\rho}\frac{v_r}{r^2}+\frac{2}{3}\frac{1}{r}\frac{\mu}{\rho}(\nabla.\vec{v}) \tag{3}$$

where

$$(\nabla.\vec{v})=\frac{\partial v_x}{\partial x}+\frac{\partial v_r}{\partial r}+\frac{v_r}{r} \tag{4}$$

Energy equation:

$$\frac{\partial(v_xT)}{\partial x}+\frac{\partial(v_rT)}{\partial r}=\frac{1}{\rho}\left(\frac{\partial}{\partial x}\left(\Gamma\frac{\partial T}{\partial x}\right)+\frac{\partial}{\partial r}\left(\Gamma\frac{\partial T}{\partial r}\right)\right) \tag{5}$$

where x and r are the axial and radial coordinates respectively, v_x and v_r are the respective axial and radial velocity, T is the temperature, Γ is the exchange coefficient for general transport, ρ is the

density, p is the pressure and μ is the dynamic viscosity of nanofluid. For turbulent flow regime, both the terms Γ and μ are replaced by their effective values and defined as

$$\mu_{eff} = \mu + \mu_t \tag{6}$$

$$\Gamma_{eff} = \frac{\mu}{Pr} + \frac{\mu_t}{\sigma_t} \tag{7}$$

respectively, where μ_t is the turbulent molecular viscosity, σ_t is the constant of turbulent Prandtl number and *Pr* is the Prandtl number of nanofluid.

4. Turbulent modeling

Realizable $\kappa - \epsilon$ turbulent model was proposed by Shih *et al.* [33], which is used in the present numerical investigation because it differs from the standard $\kappa - \epsilon$ model in two important ways. Firstly, the realizable $\kappa - \epsilon$ model includes a new formulation for the turbulent viscosity and secondly, a new transport equation for the dissipation rate is drawn from an exact equation for the transport of the mean-square vorticity fluctuation [32]. To justify the use of realizable $\kappa - \epsilon$ turbulent model in the present analysis, following investigation is initially carried out.

Three different turbulent models such as realizable $\kappa - \epsilon$ turbulent model, standard $\kappa - \epsilon$ turbulent model and RNG $\kappa - \epsilon$ turbulent model are used to see the variation of fully developed turbulent kinetic energy profile for *Re* = 21800 and *Pr* = 7.04 as shown in Fig. 2. These profiles are compared with the experimental result of Schildknecht *et al.* [34] as well as different $\kappa - \epsilon$ models suggested by Launder and Sharma [35], Chien [36] and Fan *et al.* [37]. It is clearly understood that the realizable $\kappa - \epsilon$ turbulent model performs better than the other two $\kappa - \epsilon$ turbulent models.

The equations for the turbulent kinetic energy (κ) and dissipation rate of turbulent kinetic energy (ϵ) used in the realizable $\kappa - \epsilon$ turbulent model are given by

$$div(\rho\kappa\vec{v}) = div\left\{\left(\mu + \frac{\mu_t}{\sigma_k}\right) grad\ \kappa\right\} + G_\kappa - \rho\epsilon \tag{8}$$

$$div(\rho\epsilon\vec{v}) = div\left\{\left(\mu + \frac{\mu_t}{\sigma_\epsilon}\right) grad\ \epsilon\right\} + \rho C_1 S_\epsilon - \rho C_2 \frac{\epsilon^2}{\kappa + \sqrt{\nu\epsilon}} \tag{9}$$

where $$C_1 = max\left[0.43, \frac{\eta}{\eta + 5}\right],\ \eta = S\frac{\kappa}{\epsilon}\ \text{ and }\ S = \sqrt{2\, S_{ij}\, S_{ij}} \tag{10}$$

In these equations, G_κ represents the generation of turbulence kinetic energy due to the mean velocity gradients, determined from $\mu_t\, S^2$ where, *S* is the modulus of the mean rate-of-strain tensor, σ_κ and σ_ϵ are the effective Prandtl numbers for turbulent kinetic energy and rate of dissipation, respectively; and μ_t is modelled as

$$\mu_t = \frac{\rho\kappa^2}{\epsilon}\left(A_0 + A_s\frac{\kappa U^*}{\epsilon}\right)^{-1} \tag{11}$$

where A_0 and A_s are the model constants given as $A_0 = 4.04$ and $A_s = \sqrt{6cos\phi}$ respectively with $\phi = \left(3cos^{-1}\sqrt{6W}\right)^{-1}$ and the formulations for U^* and W depend on the angular velocity. In Eqs. (8) and (9), the model constants are $C_2 = 1.9,\ \sigma_\kappa = 1.0$ and $\sigma_\epsilon = 1.2$. Further information is available in Fluent [32] for turbulent modelling.

5. Boundary conditions

The set of governing partial differential equations are non-linear and coupled. Hence, the solution of the system of nonlinear partial differential equations depends on suitable boundary conditions and thus following boundary conditions are used. At the pipe inlet, uniform velocity $v_{x,in}$ as well as uniform temperature $T_{in} = 293\ K$, turbulent intensity $I = 0.16\ Re^{-1/8}$ and hydraulic diameter, $D_h = 0.019\ m$ have been stated. All the thermal properties calculation is taken at T_{in} which is also considered as a reference temperature. For the prediction of flow in a circular pipe, the Reynolds number is defined as

$$Re = \frac{v_m D_h}{\nu} \tag{12}$$

where v_m is the mean fluid velocity defined as

$$v_m = \frac{2}{R^2}\int_0^R v(r,x)\ r\ dr \tag{13}$$

where ν is the kinematic viscosity of the nanofluid, $v(r,x)$ is the axial velocity profile and R is the radius of the pipe.

At the pipe outlet, a static gauge pressure, $p_{gauge} = 0$ is specified and the solver extrapolates the other flow and scalar quantities such as temperature and turbulent quantities from the interior domain. Note that the length of the pipe considered is sufficiently large for the flow and temperature fields to develop fully by the outlet section. On the pipe wall, a no-slip boundary condition is introduced and uniform heat flux boundary condition has been implemented.

Enhanced wall treatment is a near-wall modelling method that combines a two-layer model with enhanced wall functions. If the near-wall mesh is fine enough to be able to resolve the laminar sublayer, then the enhanced wall treatment will be identical to the traditional two-layer model. However, the restriction that the near-wall meshes must be sufficiently fine everywhere which might impose to large computational requirement. Ideally, then, one would like to have a near-wall formulation that can be used with coarse meshes as well as fine meshes. In addition, excessive error should not be incurred for intermediate meshes that are too fine for the near-wall cell centroid to lie in the fully turbulent region, nor too coarse to properly resolve the sublayer [32]. That's why, in the present analysis, enhanced wall treatment is used.

6. Nanofluids physical properties

It's not easy to evaluate the thermophysical properties in nanofluids, because we don't know which models will give us reliable results and also the solutions are strongly affected by them. Different types of models for nanofluids thermophysical properties have been presented and published by many researchers. Nevertheless, categorisation of thermophysical properties of nanofluids are still remain a subject of debate and no conclusion has been made for flow and heat transport applications because of its variety and intricacy. In the present analysis, thermophysical properties of density and heat

capacitance of the nanofluid are calculated by using following formulas which are considered as classical relationships between the base fluid and nanoparticles, Buongiorno [38].

6.1 Density

The density of the nanofluid is defined as

$$\rho_{nf} = (1-\chi)\rho_f + \chi\rho_p \tag{14}$$

where χ is the nanoparticles volume concentration, ρ_f and ρ_p are the density of the base fluid and nanoparticles respectively.

6.2 Specific heat

The heat capacitance of the nanofluid is defined as

$$(\rho c_p)_{nf} = (1-\chi)(\rho c_p)_f + \chi(\rho c_p)_p \tag{15}$$

where $(\rho c_p)_f$ and $(\rho c_p)_p$ are the heat capacitance of the base fluid and nanoparticles respectively.

6.3 Thermal conductivity

Because of lack of experimental results and correlations which depend on the nanoparticle size diameter as well as temperature, in relation to the thermophysical properties of nanofluid, the following correlations proposed by Corcione [39] are used in our analysis.

Corcione [39] introduced the following correlation to examine the thermal conductivity of nanofluid which depends on the temperature and volume concentration of nanofluid, size diameter and thermal conductivity of nanoparticles and also the base fluid. He used regression analysis and proposed the following correlation with 1.86% standard deviation of error:

$$\frac{\lambda_{nf}}{\lambda_f} = 1 + 4.4\, {Re_p}^{0.4} {Pr_f}^{0.66} \left(\frac{T}{T_{fr}}\right)^{10} \left(\frac{\lambda_p}{\lambda_f}\right)^{0.03} \chi^{0.66} \tag{16}$$

where, Re_p is the nanoparticles Reynolds number, defined as

$$Re_p = \frac{\rho_f u_B\, d_p}{\mu_f} = \frac{2\rho_f\, \kappa_b\, T}{\pi\, {\mu_f}^2 d_p} \tag{17}$$

Here T_{fr} is the freezing point of the base liquid (273.16 K), κ_b is the Boltzmann constant ($\kappa_b \approx 1.38 \times 10^{-23}\, J/K$), d_f is the fluid molecular diameter, d_p is the diameter of nanoparticles ($10\ \text{nm} \leq d_p \leq 150\, nm$), T is the nanofluid temperature ($294 \leq T(K) \leq 324$), χ is a particle volume concentration which is valid for $0.2\% \leq \chi \leq 9\%$, Pr_f is the Prandtl number of the base fluid, ρ_f and μ_f are the density and the dynamic viscosity of the base fluid, respectively, and u_B is the nanoparticle Brownian velocity which is calculated as the ratio between d_p and the time $\tau_D = {d_p}^2/6D$ by assuming the absence of agglomeration. Here *D* is the Einstein diffusion coefficient.

6.4 Dynamic viscosity

Corcione [39] proposed another correlation to evaluate the dynamic viscosity of nanofluid. He used best-fit of the selected data specified in his research work and proposed the following correlation with 1.84% standard deviation of error:

$$\frac{\mu_f}{\mu_{nf}} = 1 - 34.87 \left(\frac{d_p}{d_f}\right)^{-0.3} \chi^{1.03} \tag{18}$$

where d_p is the diameter of nanoparticles ($25\ \text{nm} \leq d_p \leq 200\ nm$), χ is a particle volume concentration which is valid for $0.01\% \leq \chi \leq 7.1\%$, T is the nanofluid temperature ($293 \leq T(K) \leq 333$) and d_f is the base fluid molecular diameter defined by

$$d_f = 0.1 \left(\frac{6M}{N\pi\rho_f}\right)^{1/3} \tag{19}$$

in which N is the Avogadro number and M is the molecular weight of the base fluid.

The above correlations are derived from an extensive selection of empirical data relative to nanofluids consisting of different mean diameter of nanoparticles, suspended in water (H_2O) or Ethylene glycol (EG) for the development of thermal conductivity correlation and water (H_2O), propylene glycol (PG), Ethylene glycol (EG) or ethanol (Eth) for the development of dynamic viscosity correlation. It is to be noted that the conventional Maxwell theory mostly fails when implemented to nanofluids. In reality, the conventional Maxwell equation tends either to underestimate or to overestimate the value of thermal conductivity of nanofluid, according as the nanoparticle diameter is small or large, respectively and the temperature of the suspension is high or low, respectively as discussed in Corcione [39]. Also the Brinkman equation mostly fails when implemented to nanofuids, with a percentage error that increases as the size diameter of nanoparticles decreases. It should also be noted that for the calculation of dynamic viscosity of nanofluid with nanoparticles size diameter of 10 and 20 nm, this model is used in this study by assuming a possible standard deviation of error higher than 1.84%.

7. Thermophysical properties of the base fluid and nanoparticles

The mass density, heat capacitance, kinematic viscosity and thermal conductivity of the base fluid (water) were calculated using the following correlations proposed by Kays and Crawford [40]. All these correlations are valid over $278 \leq T(K) \leq 363$.

$$\rho_f = 330.12 + 5.92\,T - 1.63 \times 10^{-2} T^2 + 1.33 \times 10^{-5} T^3 \tag{20}$$

$$C_{p_f} = 10^{-3} \times (10.01 - 5.14 \times 10^{-2}\,T + 1.49 \times 10^{-4}\,T^2 - 1.43 \times 10^{-7}\,T^3) \tag{21}$$

$$\nu_f = 1.08 \times 10^{-4} - 9.33 \times 10^{-7}\,T + 2.70 \times 10^{-9}\,T^2 - 2.62 \times 10^{-12}\,T^3 \tag{22}$$

$$\lambda_f = -12.16 + 0.12\,T - 3.66 \times 10^{-4}\,T^2 + 3.81 \times 10^{-7}\,T^3 \tag{23}$$

The density, heat capacitance and thermal conductivity of Al_2O_3 at T = 293 K is considered as Masuda *et al.* [41]: $\rho_p = 3880 \frac{kg}{m^3}$, $C_{p_p} = 773\ \frac{J}{kgK}$, $\lambda_p = 36\ \frac{W}{mK}$

The thermal conductivity of TiO_2 is obtained from the following relation and designed by curve fitting on the data of Powel *et al.* [42]:

$$\lambda_p = 100 \times (0.1813 - 4.768 \times 10^{-4}\,T + 5.089 \times 10^{-7}\,T^2), \quad \text{where } 273 \leq T(K) \leq 350 \tag{24}$$

The heat capacitance of TiO_2 is obtained from the following relation and designed by curve fitting on the data of Smith *et al.* [43]:

$$C_{p_p} = 58.4528 + 3.02195\,T - 3.02923 \times 10^{-3}\,T^2, \quad \text{where } 269.35 \leq T(K) \leq 339.82 \tag{25}$$

The density of TiO_2 is considered as $4250\,\frac{kg}{m^3}$.

8. Numerical methods

The computational domain is formed by using the commercial pre-processor software GAMBIT 2.4.6 which is also used for meshing and setting the boundary conditions. Then the governing non-linear partial differential equations for the continuity, momentum, energy and other scalars such as turbulence together with the suitable boundary conditions are discretised and hence solved by using the Finite volume solver Fluent 6.3.26. The finite volume technique converts the non-linear partial differential equations with the second order upwind scheme to a system of nonlinear algebraic equations that are solved numerically. Second order upwind scheme is employed to achieve higher-order accuracy at the cell faces through a Taylor series expansion of the cell-centred solution about the cell centroid. The pressure-based solver employed to solve the pressure based equation which is derived from the momentum and continuity equations. All these equations are solved sequentially and iteratively so as to obtain a converged numerical solution. For all the simulations carried out in the present analysis, convergence criteria for the solutions are considered when the residuals become less than 10^{-6}.

9. Grid sensitivity analysis

In order to justify the correctness as well as the stability of the numerical findings, extensive computations have been performed to determine the total number of grid points that generate a suitable arrangement result which will be appropriate to determine the flow and thermal field in a pipe. The grid sensitivity study is carried out by varying the total number of grid distributions in both the radial *(Nr)* and axial *(Nx)* directions. For a particular test case of the base fluid water of Prandtl number, $Pr = 7.04$ and Reynolds number, $Re = 100 \times 10^3$, various combinations of grid have been analysed to justify that the numerical results are grid independent. Figure 3 shows the variation of radial velocity, temperature and turbulent kinetic energy profiles at the fully developed location (x = 0.9 m) near the outlet. It can be seen that the grids 500×100, 500×150 and 1000×100 generate most reasonable results as the differences found among the results are insignificant. Therefore, the selected grid for the present calculations consisted of 500 and 100 nodes respectively along the axial and radial directions to save the computational time and to avoid any inconsistencies in the numerical results. In addition, to capture the large variations of flow field behaviour near the inlet and pipe wall, uniform grid in the axial direction and non-uniform grid in the radial direction are considered.

10. Validation of the present numerical results

10.1 Water

In order to validate the accurateness of the present numerical findings, firstly the radial velocity and turbulent kinetic energy profile for *Re* = 21800 and *Pr* = 7.04 which are taken at the fully developed section near the outlet are validated against the experimental result of Schildknecht *et al.* [34] as well as with different κ-ϵ models suggested by Launder and Sharma [35], Chien [36], Fan *et al.* [37], Jones and Launder [44, 45], Lai and So [46] and Myong and Kasagi [47]. These researchers have used the following model to determine the turbulent kinematic viscosity with the model constants summarised in Table 1.

$$\nu_T = C_\mu f_\mu \frac{\kappa^2}{\epsilon} \tag{26}$$

where f_μ is a damping function.

Table 1: Model constants

Researchers	C_μ	C_1	C_2	σ_κ	σ_ϵ
Launder and Sharma [35]	0.09	1.44	1.92	1.0	1.3
Chien [36]	0.09	1.35	1.8	1.0	1.3
Fan *et al.* [37]	0.09	1.40	1.8	1.0	1.3
Jones and Launder [44, 45]	0.09	1.45	2.0	1.0	1.3
Lai and So [46]	0.09	1.35	1.8	1.0	1.3
Myong and Kasagi [47]	0.09	1.40	1.8	1.4	1.3

In Figure 4, radial velocity and turbulent kinetic energy are nondimensionalised by fiction velocity, u_τ and then presented. From Fig. 4(a), it can be seen that the non-dimensional velocity profile shows good agreement with the models proposed by Launder and Sharma [35], Chien [36] and Fan *et al.* [37]. It is also found that the present result differs from the models proposed by Jones and Launder [44, 45] and Lai and So [46] as well as the experimental result of Schildknecht *et al.* [34]. In fact, a significant variation is observed between all the models as well as the present result with the experimental result. The reason behind this fact may be the over estimation of the maximum mean velocity obtained from the experimental result. Among all the results, Jones and Launder [44, 45] show the poorest prediction of the non-dimensional velocity profile.

Further, it is seen that the highest value of turbulent kinetic energy founds at some radial location near the wall. It is also seen that this radial location does not differ extensively among the experimental and numerical results as shown in Fig. 4(b). It is found that most of the models proposed by the different researchers predicted relatively good value of the magnitude of highest turbulent kinetic energy compared with the experimental result. But the findings of Jones and Launder [44, 45], Launder and Sharma [35] and also the present result show an under prediction of the maximum peak intensity. This may be due to the different models for the turbulent viscosity as well as different model constants and damping functions used by the researchers.

Additional validation has been done against the existing correlations for different *Re* = 10×10^3 to 100×10^3 and *Pr* = 7.04. In order to perform the validation, numerical results of Darcy friction factor

are compared with the correlations suggested by Blasius [48] and Petukhov [49] and also, average Nusselt number are compared with the correlations proposed by Petukhov [49], Notter and Rouse [50] and Gnielinski [51] which are given as follows:

Blasius equation:

Blasius [48] proposed the following relation for the calculation of friction factor for pure fluid which is expressed as

$$f = \frac{0.316}{Re^{0.25}}, 3000 \le Re \le 10^5 \tag{27}$$

Petukhov [49] equation:

$$\overline{Nu} = \frac{\frac{f}{8} Re\, Pr}{1.07 + 12.7\left(\frac{f}{8}\right)^{0.5}\left(Pr^{\frac{2}{3}} - 1\right)}, \begin{pmatrix} 0.5 \le Pr \le 2000 \\ 10^4 \le Re \le 5 \times 10^6 \end{pmatrix}$$
$$f = (0.79 \ln Re - 1.64)^{-2}, 10^4 \le Re \le 5 \times 10^6 \tag{28}$$

Notter-Rouse Equation:

Notter and Rouse [50] introduced the following correlation for the calculation of average Nusselt number for pure fluid:

$$\overline{Nu} = 5.0 + 0.015\, Re^{0.856} Pr^{0.347} \tag{29}$$

Gnielinski [51] equation:

$$\overline{Nu} = \frac{\frac{f}{8} (Re - 1000)\, Pr}{1.0 + 12.7\left(\frac{f}{8}\right)^{0.5}\left(Pr^{\frac{2}{3}} - 1\right)}, \begin{pmatrix} 0.5 \le Pr \le 2000 \\ 3000 < Re \le 5 \times 10^6 \end{pmatrix}$$
$$f = (1.82 \ln Re - 1.64)^{-2}, 10^4 \le Re \le 5 \times 10^6 \tag{30}$$

Figure 5(a) shows compatible results of the Darcy friction factor between the present numerical result on the base fluid and other correlations of Blasius [48] and Petukhov [49]. Maximum deviation of 8.91% for $Re = 20 \times 10^3$ and minimum deviation of 3.47% are observed for $Re = 100 \times 10^3$. This may be due to the higher pressure drop obtained for different *Re* in the present simulation.

Also, the result of average Nusselt number is presented in Fig. 5(b). The maximum deviation between our numerical result and the correlations of Petukhov [49], Notter and Rouse [50] and Gnielinski [51] are 3.84%, 1.63% and 5.40% respectively which shows very good agreement with these correlations. It is important to note that all these available correlations are not highly accurate. The accuracy of each correlation is fully dependent on different types of application so more or less variation will occur depending on the problems. Hence, it's possible to say that percentage error of 3.84%, 1.63% and 5.40% are in very close to the acceptable region. Other factors like near wall mesh distribution and temperature gradient at the wall are also responsible for such variations.

Here we note that the Darcy friction factor and local Nusselt number are evaluated according to the following relations:

Darcy friction factor for turbulent flows in a circular pipe is defined as

$$f = \frac{2D_h \Delta p}{\rho L v_m^2} \tag{31}$$

Local Nusselt number and heat transfer coefficient are defined as

$$Nu(x) = \frac{h(x)\, D_h}{\lambda_f} \; where \; h(x) = \frac{\dot{q}_s}{T_w - T_m(x)} \; and \; \dot{q}_s = -\lambda_f \left.\frac{\partial T}{\partial r}\right|_{r=R} \tag{32}$$

Also, for constant and uniform heat flux boundary condition, the mean temperature of a fluid flowing through a circular pipe is expressed as

$$T_m(x) = T_{m,i} + \frac{\dot{q}_s \pi D_h}{\dot{m} C_p} x \tag{33}$$

where $\dot{q}_s \; and \; \dot{m}$ are the heat flux of the pipe and mass flow rate of the fluid, respectively.

From the above equations, the average Nusselt number is defined as

$$\overline{Nu} = \frac{1}{L} \int_0^L Nu(x)\, dx \tag{34}$$

This numerical integration has been performed by using the Simpson's 1/3 rule.

10.2 Al_2O_3-Water nanofluid

From the comparisons presented in the section above, we can conclude that our computational model is producing the correct outcomes; hence Al_2O_3-H_2O nanofluid flow in a circular pipe with different $\chi = 0.01, 0.04$ and 0.06 is now investigated for different $Re = 10 \times 10^3$ to 100×10^3 with $7.04 < Pr < 10.0$. Also, in the present analysis, heat flux $\dot{q}_s = 50 \times 10^3$ W/m^2 is considered [26, 27] which is applied on the pipe wall. Then a comparison is made between the present computed Nusselt number and the Pak and Cho [52] correlation. Also, for the validation purpose, the following correlations are used to model the dynamic viscosity as well as thermal conductivity of Al_2O_3-H_2O nanofluid.

$$\mu_{nf} = \mu_f (123\, \chi^2 + 7.3\, \chi + 1) \tag{35}$$

$$\lambda_{nf} = \lambda_f (4.97\, \chi^2 + 2.72\, \chi + 1) \tag{36}$$

Eq. (35) is derived from the experimental data of Masuda *et al.* [41], Lee *et al.* [53] and Wang *et al.* [54] by using least square curve fitting. Other classical models like Einstein [55] or Brinkman [56] can be used but it is found that these models underestimate the dynamic viscosity of nanofluid as shown by Maiga *et al.* [57]. Also, Eq. (36) is developed using the model suggested by Hamilton and Crosser [58] with the assumption that nanoparticles are spherical in size and shape and then implemented in this work because of its simplicity.

Pak and Cho [52] investigated experimentally the heat transfer behaviours of nanofluids in a circular pipe under turbulent flow regime. Investigation was carried out for Al_2O_3-H_2O and TiO_2-H_2O nanofluids, *Re* and *Pr* were varied in the ranges from 10^4 to 10^5 and 6.5 to 12.3 respectively. They have established the following correlation only depending on *Re* and *Pr* and this correlation does not depends on χ as well as nanoparticles size diameter.

$$\overline{Nu} = 0.021 Re^{0.8} Pr^{0.5} \tag{37}$$

In Figure 6, a comparison between the present result and that of Pak and Cho [52] is shown graphically for the Al_2O_3-H_2O nanofluid and $\chi = 0.01, 0.04$ and 0.06. It is found that the present numerical findings are in very good agreement with the results of Pak and Cho [52] which is completely empirical referred by Buongiorno [38]. Although Eq. (37) developed using Al_2O_3-H_2O

and TiO_2-H_2O nanofluids, this correlation should be applicable in general (Das *et al.* [59]). It is also crucial to note that Eq. (37) was valid for relatively low nanoparticle volume concentration, say e.g. when $\chi \leq 3.2\%$ but we considered the trend and apply this for higher χ by assuming the higher standard deviation of error.

11. Results and discussion

The numerical investigations are performed using Al_2O_3-H_2O and TiO_2-H_2O nanofluids, with the subsequent choices of parameters: the Reynolds number from $Re = 10 \times 10^3$ to 100×10^3, Prandtl number from 7.04 to 20.29, the particle volume concentration of 4% and 6% and diameter of the nanoparticles of $10, 20, 30$ and $40\ nm$. The outcomes are presented hereafter focusing on the impacts of nanoparticle volume concentration, Brownian motion and size diameter of Al_2O_3 and TiO_2 nanoparticles and different Reynolds number on the hydrodynamic flow and thermal performance of the nanofluids under the turbulent flow condition.

11.1 Fully developed velocity profile

Figure 7 displays the effect of various volume concentrations, different nanoparticles size diameter of Al_2O_3-water nanofluid on the fully developed velocity profile for $Re = 100 \times 10^3$. In general, the kinematic viscosity of nanofluid is always higher than the base fluid and hence the velocity of nanofluid always possesses higher value compared to the base fluid. Similarly, as the nanoparticle size decreases from 40 to 10 *nm*, the kinematic viscosity increases with the nanoparticle volume concentration. From this observation, it can be observed that the maximum peak value of the velocity found is highest for d_p = 10 *nm* and χ = 6% then decreases with the increase of mean diameter of nanoparticles. Similar behaviour is observed for all the Reynolds numbers as well as the TiO_2-water nanofluid. It should be noted that for different nanoparticles size diameter and volume concentration, the maximum velocity varies significantly at the centreline position.

11.2 Turbulent kinetic energy profile

Figure 8 shows the effect of various volume concentrations, different nanoparticle size diameters of Al_2O_3-water nanofluid on the turbulent kinetic energy for $Re = 100 \times 10^3$. It can be seen that when the particle volume concentration is changed from 4% to 6% of the Al_2O_3-water nanofluid, the radial location at which the highest value of the turbulent kinetic energy appears does not differ considerably for the different nanoparticles size diameter and the maximum peak value of κ is observed for d_p = 10 *nm*. Similar behaviour is observed for all the Reynolds numbers as well as for the TiO_2-water nanofluid. It should be noted that as the nanoparticles size diameter increases from 10 to 40 *nm*, the maximum peak value of κ rapidly decreases which shows the lower turbulent intensity near the surface and therefore, the turbulent strength in the flow tends to reduce. This result further indicates that the smaller diameter of nanoparticle plays an important role in turbulence generation compared to that by the large diameter of nanoparticle. The reason behind this fact may be due to the Brownian motion as well as the shape and size of the nanoparticles.

11.3 Average shear stress coefficient ratio

Figure 9 shows the effect of various nanoparticle volume concentrations, different nanoparticle size diameters of water based Al_2O_3 and TiO_2 nanofluids on the average shear stress ratio, defined as the ratio of the average shear stresses, $\overline{\tau_\tau} = \overline{\tau_{nf}}/\overline{\tau_f}$. From this investigation, it is found that the average shear stress ratio has increased with the increase of nanoparticle volume concentration and decrease of nanoparticle size diameter of 40 to 10 *nm* and such enhancement is independent to the Reynolds number. In particular, for *Re* = 20×10^3 and Al_2O_3-water nanofluid, $\overline{\tau_\tau}$ has a value of 2.0, 2.19, 2.54 and 3.58 for $\chi = 4\%$ and d_p = 40, 30, 20 and 10 *nm* respectively. Also, for higher particle volume concentration, e.g. $\chi = 6\%$, $\overline{\tau_\tau}$ has a value of 3.42, 4.13, 5.79 and 14.63 for d_p = 40, 30, 20 and 10 *nm* respectively. Similar performances have also been noticed for the TiO_2-water nanofluid. From the above findings, it is possible to conclude that the increase of the average shear stress ratio with respect to the nanoparticle volume concentration as well as the nanoparticle size diameter emerge to be noticeably more significant for both the water based Al_2O_3 and the TiO_2 nanofluids. Such enhancement of the average shear stress ratio may be due to the adverse effects of increase frictional force or pressure.

11.4 Heat transfer analysis

Figure 10 shows the effect of various volume concentrations, different nanoparticles size diameter of water based Al_2O_3 and TiO_2 nanofluids along with the results of the base fluid on the average Nusselt number. It can be seen that the average heat transfer rate increases with the increase of Reynolds number, nanoparticle volume concentration when the nanoparticle size diameter changes from 40 *nm* to 10 *nm*. Also it is found that the average heat transfer rate of the water based Al_2O_3 and TiO_2 nanofluids is higher than that of the base fluid at any Reynolds number. The explanation for such augmentation in the average heat transfer rate may be associated to different aspects such as enhancement of thermal conductivity, nanoparticle size and shapes, Brownian motion of particles, decrease in boundary layer thickness and delay in boundary layer growth.

The average Nusselt number is very responsive to types and diameter of the nanoparticles, as observed. From our investigation, it is examined that the effect of average heat transfer rate increases with the decrease of nanoparticle size diameter. For example, for the Al_2O_3–water nanofluid and χ = 4% and 6% with d_p = 10 *nm*, the maximum enhancement is approximately 21.75% and 59.83% respectively while for d_p = 20 *nm*, the maximum enhancement is approximately 14.34% and 33.60% respectively. However, for the TiO_2–water nanofluid and χ = 4% and 6% with d_p = 10 *nm*, the maximum enhancement is approximately 21.28% and 58.79% respectively while for d_p = 20 *nm*, the maximum enhancement is approximately 13.80% and 32.79% respectively. Similar trend is observed as nanoparticle size diameter increases from 20 *nm* to 30 *nm* or 30 *nm* to 40 *nm*. In order to achieve a higher heat transfer rate, 10 *nm* diameter size particles is best for both water based Al_2O_3 and TiO_2

nanofluids. It can also be observed that Al_2O_3–H_2O nanofluid gives us slightly better heat transfer rate than the TiO_2– H_2O nanofluid for all the Reynolds numbers, nanoparticle volume concentration as well as nanoparticles size diameter. Values of maximum increment in the average heat transfer rate of water based Al_2O_3 and TiO_2 nanofluids are shown in Table 2 for different nanoparticles size diameter and volume concentration.

From Figure 10, it is observed that smaller diameter and Brownian motion of nanoparticles assist to increase the viscosity for same particle volume concentration and hence make an impact on the Nusselt number enhancement. This is quite reasonable because smaller nanoparticles with higher velocity move faster than the large particles thus reduce the possibility of collision with each other. Also, smaller diameter of nanoparticles will be more in number compare to large diameter of nanoparticles and will make a contact with the neighbouring fluid over a greater surface area. It will help in increasing the viscosity and thermal conductivity of water based Al_2O_3 and TiO_2 nanofluids which result in the enhancement of heat transfer.

Table 2: Maximum increment (%) of average Nusselt number for different nanofluids

	Al_2O_3-water		TiO_2-water	
d_p *(nm)*	χ = 4%	χ = 6%	χ = 4%	χ = 6%
10	21.75	59.83	21.28	58.79
20	14.34	33.60	13.83	32.79
30	11.27	25.14	10.75	24.30
40	09.45	20.63	08.90	19.78

11.5 Thermal performance factor

Thermal performance factor is defined as follows (Suresh *et al*. [60]):

$$\xi = \left(\frac{\overline{Nu}_{nf}}{\overline{Nu}_f}\right)\left(\frac{f_{nf}}{f_f}\right)^{\frac{1}{3}} \tag{38}$$

Figure 11 shows the thermal performance factor which is investigated with the use of various volume concentrations of 4% and 6%, different nanoparticle size diameters of 10 to 40 *nm* and water based Al_2O_3 and TiO_2 nanofluids. It is observed that the value of the thermal performance factor remains greater than one for all the possible cases considered and it is very close to the ratio of the average heat transfer rate of nanofluid and base fluid. Also, it is further observed that the ratio of Darcy friction factor of nanofluid and base fluid is approximately close to 1. Hence it is possible to make a conclusion that the heat transfer enhancement is possible with little or without penalty in the pumping power. This may lead to less energy cost and more efficient for practical application. From the above investigation, it is also evident that the thermal performance factor increases as the nanoparticle volume concentration increases and higher values of ξ is achieved for smaller nanoparticle size diameter for water based Al_2O_3 and TiO_2 nanofluids. Another reason might be that as the nanoparticles size diameter decreases from 40 to 10 *nm*, the dynamic viscosity and thermal conductivity of nanofluid increases with the increase of nanoparticle volume concentration. Hence the higher viscosity directs to a diminution of boundary layer thickness resulting in the enhancement of

heat transfer whereas the higher thermal conductivity directs to an intensification of thermal performance factor.

11.6 Correlations

In the present analysis, the following correlations have been proposed for the calculation of average Nusselt number using the non-linear regression analysis and the average Nusselt number is the function of Reynolds number, Prandtl number and nanoparticles size diameter. It is to be noted that these correlations are valid when the Brownian motion of nanoparticles is taken into account. Also, the values of maximum standard deviation of error are 7.35% and 7.25% for Al_2O_3 and TiO_2 nanofluids respectively. Further, comparisons between the numerical results of average Nusselt number and computed by the proposed correlations are presented in Fig. 12. This Figure shows a good agreement between the numerical results and the proposed correlations.

Al_2O_3-H_2O nanofluid : $$\overline{Nu} = 0.01272\, Re^{0.85861} Pr^{0.42986} \left(\frac{d_f}{d_p}\right)^{-0.00017} - 0.5 \quad (39)$$

TiO_2-H_2O nanofluid : $$\overline{Nu} = 0.01259\, Re^{0.85926} Pr^{0.43020} \left(\frac{d_f}{d_p}\right)^{-0.00068} \quad (40)$$

where

$10 \times 10^3 \leq Re \leq 100 \times 10^3,\ 8.45 \leq Pr \leq 20.29,\ 10 \leq d_p(nm) \leq 40,\ 4 \leq \chi(\%) \leq 6.$

12. Conclusion

In this research work, numerical investigations have been carried out to understand the flow and heat transfer behaviour of different nanofluids in a horizontal circular pipe under turbulent flow condition. The effects of Reynolds number and Prandtl number, two different nanofluids, nanoparticle volume concentration, diameter size and Brownian motion of nanoparticles on flow and heat transfer are investigated. According to our findings, following conclusion can be made and summarised as follows:

(a) It was found that for χ = 4% and 6%, water based Al_2O_3 and TiO_2 nanofluids with 10 to 40 *nm* particles size diameter with Brownian motion of nanoparticles, average Nusselt number and shear stress ratio are significantly higher compared to the base fluid.

(b) It was investigated that the water based Al_2O_3 and TiO_2 nanofluids with 10 *nm* and χ = 6% show higher thermal performance factor for any Reynolds number and nanoparticles size diameter.

(c) It was observed that the friction factor of nanofluids has no significant effect compared to the base fluid and hence induce no extra penalty in pump power.

Furthermore, we have found that the Al_2O_3-H_2O nanofluid shows slightly better heat transfer performance than that of the TiO_2-H_2O nanofluid. But since TiO_2 nanoparticles are more environment-friendly and eco-friendly [61] than the Al_2O_3 nanoparticles, hence it is better to use TiO_2-water nanofluid in real life application. Also, it was seen that the heat transfer performance is more influenced by the Brownian motion and size diameter of nanoparticles than the thermal conductivity of nanofluid.

Nomenclature

A_0, A_1, C_1, C_2, C_μ	Model constant	v	Velocity (m/s)
C_p	Specific heat capacity ($J/kg\ K$)	x	Axial coordinate (m)
D	Einstein diffusion coefficient	*Greek symbols*	
D_h	Diameter of a pipe (m)	ρ	Density (kg/m^3)
d_f	Fluid molecular diameter (m)	μ	Dynamic viscosity (kg/ms)
d_p	Diameter of nanoparticle (nm)	λ	Thermal conductivity ($W/m\ K$)
f	Darcy friction factor	κ	Turbulent kinetic energy (m^2/s^2)
f_μ	Dumping function	μ_t	Turbulent molecular viscosity
G_k	Generation of turbulent kinetic energy	ϵ	Dissipation rate of Turbulent kinetic energy (m^2/s^3)
I	Turbulent intensity	χ	Nanoparticle volume concentration
L	Length (m)	ξ	Thermal performance factor
M	Molecular weight of the base fluid	τ_D	Time (s)
$\dot{m}$	Mass flow rate (kg/s)	$\overline{\tau_\tau}$	Ratio of average shear stresses
N	Avogadro number	Γ	Exchange coefficient for general transport
N_x, N_r	Number of grid distribution in axial and radial directions	σ_t	Constant of turbulent Prandtl number
Nu	Local Nusselt number	σ_κ	Effective Prandtl number for turbulent kinetic
$\overline{Nu}$	Average Nusselt number	σ_ϵ	Effective Prandtl number for rate of dissipation
p	Pressure (N/m^2)	*Subscripts*	
Pr	Prandtl number	in	Inlet
$\dot{q}_s$	Heat flux of the pipe (W/m^2)	f	Base fluid
R	Radius of a pipe (m)	nf	nanofluid
Re	Reynolds number	p	nanoparticle
r	Radial coordinate (m)	w	Wall
S	Modulus of the mean rate of strain tensor	m	Mean
T	Temperature (K)	eff	Effective
T_{fr}	Freezing point of the base fluid (K)		
T_w	Temperature at the wall (K)		
T_m	Mean temperature of a fluid (K)		
u_B	Nanoparticle particle mean Brownian velocity (m/s)		
u_τ	Friction velocity (m/s)		
V_m	Mean fluid velocity (m/s)		

References

[1] S.P. Jang, S.U.S. Choi, Cooling performance of a microchannel heat sink with nanofluids, Applied Thermal Engineering, 26 (2006) 2457–2463.

[2] D. Singh, J. Toutbort, G. Chen, Heavy vehicle systems optimization merit review and peer evaluation, in, Argonne National Laboratory, 2006.

[3] J.C. Nelson, D. Banerjee, R. Ponnappan, Flow loop experiments using polyalphaolefin nanofluids, Journal of Thermophysics and Heat Transfer 23 (2009) 752-761.

[4] D.P. Kulkarni, D.K. Das, R.S. Vajjha, Application of nanofluids in heating buildings and reducing pollution, Applied Energy 86 (2009) 2566–2573.

[5] J. Buongiorno, L.W. Hu, S.J. Kim, R. Hannick, B. Truong, E. Forrest, Nanofluids for enhanced economics and safety of nuclear reactors: An evaluation of the potential features, issues, and research gaps, Nuclear Technology 162 (2008) 80-91.

[6] S.M. You, J.H. Kim, K.H. Kim, Effect of nanoparticles on critical heat flux of water in pool boiling heat transfer, Applied Physics Letters 83 (2003) 3374-3376.

[7] P. Vassallo, R. Kumar, S.D. Amico, Pool boiling heat transfer experiments in silica–water nano-fluids, International Journal of Heat and Mass Transfer 47 (2004) 407–411.

[8] M.F. Demirbas, Thermal energy storage and phase change materials: an overview, Energy Sources, Part B: Economics, Planning, and Policy 1(2006) 85-95.

[9] T.P. Otanicar, P.E. Phelan, R.S. Prasher, G. Rosengarten, R.A. Taylor, Nanofluid-based direct absorption solar collector, Journal of Renewable and Sustainable Energy (2010).

[10] J. Zhou, Z. Wu, Z. Zhang, W. Liu, Q. Xue, Tribological behavior and lubricating mechanism of Cu nanoparticles in oil, Tribology Letters 8(2000) 213–218.

[11] L. Vekas, D. Bica, M.V. Avdeev, Magnetic nanoparticles and concentrated magnetic nanofluids: Synthesis, properties and some applications, China Particuology 5(2007) 43–49.

[12] L. Zhang, Y. Jiang, Y. Ding, M. Povey, D. York, Investigation into the antibacterial behaviour of suspensions of ZnO nanoparticles (ZnO nanofluids), Journal of Nanoparticle Research, 9 (2007) 479–489.

[13] X. Sun, Z. Liu, K. Welsher, J.T. Robinson, A. Goodwin, S. Zaric, H. Dai, Nano-graphene oxide for cellular imaging and drug delivery, Nano Research 1(2008) 203- 212.

[14] X. Fan, H. Chen, Y. Ding, P.K. Plucinski, A.A. Lapkin, Potential of 'nanofluids' to further intensify microreactors, Green Chemistry 10 (2008) 670–677.

[15] T. Sharma, A.L.M. Reddy, T.S. Chandra, S. Ramaprabhu, Development of carbon nanotubes and nanofluids based microbial fuel cell, International journal of hydrogen energy, 33 (2008) 6749–6754.

[16] S. Choi, Enhancing thermal conductivity of fluids with nanoparticles, In Developments and Applications of Non-Newtonian Flows, ASME, FED 231/MD 66 (1995) 99–105.

[17] L. Qiang, X. Yimin, Convective heat transfer and flow characteristics of Cu-water nanofluid, Science in China (Series E) 45 (2002) 408-416.

[18] R.B. Mansour, N. Galanis, C.T. Nguyen, Effect of uncertainties in physical properties on forced convection heat transfer with nanofluids, Applied Thermal Engineering, 27 (2007) 240–249.

[19] Y. Xuan, Q. Li, Journal of Heat Transfer Journal of Heat Transfer 125 (2003) 151–155.

[20] D. Kim, Y. Kwon, Y. Cho, C. Li, S. Cheong, Y. Hwang, J. Lee, D. Hong, S. Moon, Convective heat transfer characteristics of nanofluids under laminar and turbulent flow conditions, Current Applied Physics 9(2009) 119–123.

[21] S.M. Fotukian, M.N. Esfahany, Experimental investigation of turbulent convective heat transfer of dilute γ-Al2O3-water nanofluid inside a circular tube, International Journal of Heat and Fluid Flow 31 (2010) 606–612.

[22] A.R. Sajadi, M.H. Kazemi, Investigation of turbulent convective heat transfer and pressure drop of TiO_2-water nanofluid in circular tube, International Communications in Heat and Mass Transfer, 38 (2011) 1474–1478.

[23] S. Torii, Turbulent heat transfer behavior of nanofluid in a circular tube heated under constant heat flux, Advances in Mechanical Engineering (2010) 917612: 917611-917617.

[24] L.S. Sundar, M.T. Naik, K.V. Sharma, M.K. Singh, T.C.S. Reddy, Experimental investigation of forced convection heat transfer and friction factor in a tube with Fe_3O_4 magnetic nanofluid, Experimental Thermal and Fluid Science 37 (2012) 65–71.

[25] S.E.B. Maiga, C.T. Nguyen, N. Galanis, G. Roy, T. Mare, M. Coqueux, Heat transfer enhancement in turbulent tube flow using Al_2O_3 nanoparticle suspension, International Journal of Numerical Methods for Heat and Fluid Flow, 16 (2006) 275-292.

[26] V. Bianco, O. Manca, S. Nardini, Numerical investigation on nanofluids turbulent convection heat transfer inside a circular tube, International Journal of Thermal Sciences 50 (2011) 341-349.

[27] P.K. Namburu, D.K. Das, K.M. Tanguturi, R.S. Vajjha, Numerical study of turbulent flow and heat transfer characteristics of nanofluids considering variable properties, International Journal of Thermal Sciences 48 (2009) 290–302.

[28] P. Kumar, A CFD study of heat transfer enhancement in pipe flow with Al_2O_3 nanofluid, World Academy of Science, Engineering and Technology, 81 (2011) 746-750.

[29] Y. He, Y. Mena, Y. Zhao, H. Lu, Y. Ding, Numerical investigation into the convective heat transfer of TiO_2 nanofluids flowing through a straight tube under the laminar flow conditions, Applied Thermal Engineering 29 (2009) 1965–1972.

[30] M.H. Fard, M.N. Esfahany, M.R. Talaie, Numerical study of convective heat transfer of nanofluids in a circular tube two-phase model versus single-phase model, International Communications in Heat and Mass Transfer 37 (2010) 91–97.

[31] G. Saha, M.C. Paul, Numerical study on heat transfer and entropy generation analysis of turbulent mixed convection flow of Al_2O_3-water and TiO_2-water nanofluids in a circular pipe using two-phase mixture model, (2014) (Submitted).

[32] Fluent 6.3 user guide, Fluent Inc., Lebanon, 2006.

[33] T.H. Shih, W.W. Liou, A. Shabbir, Z. Yang, J. Zhu, A new k-ϵ eddy viscosity model for high Reynolds number turbulent flows, Computational Fluids, 24 (1995) 227-238.

[34] M. Schildknecht, J.A. Miller, G.E.A. Meier, The influence of suction on the structure of turbulence in fully developed pipe flow, Journal of Fluid Mechanics, 90 (1979) 67-107.

[35] B.E. Launder, B.I. Sharma, Application of the energy-dissipation model of turbulence to the calculation of flow near a spinning disc, Letters in Heat Mass Transfer 1(1974) 131-138.

[36] K.Y. Chien, Predictions of channel and boundary layers and heat transfer along compressor and turbine blades, Numerical Methods in Heat Transfer, 19 (1982) 413-429.

[37] S. Fan, B. Lakshminarayana, M. Barnett, Low-Reynolds-number k-ϵ model for unsteady turbulent boundary-layer flows, Journal of AIAA, 31 (1993) 1777-1784.

[38] J. Buongiorno, Convective transport in nanofluids, Journal of Heat Transfer, 128 (2006) 240-250.

[39] M. Corcione, Empirical correlating equations for predicting the effective thermal conductivity and dynamic viscosity of nanofluids, Energy Conversion and Management, 52 (2011) 789-793.

[40] W.M. Kays, M.E. Crawford, Convection heat and mass transfer, 2nd ed., McGraw Hill, New York, 1980.

[41] H. Masuda, A. Ebata, K. Teramae, N. Hishinuma, Alternation of thermal conductivity and viscosity of liquid by dispersing ultra-fine particles (dispersion of Al_2O_3, SiO_2 and TiO_2 ultra-fine particles), Netsu Bussei, 40 (1993) 227-233

[42] R.W. Powell, C.Y. Ho, P.E. Liley, Thermal conductivity of selected materials, United states department of commerce, National Bureau of standards, 1962.

[43] S.J. Smith, R. Stevens, S. Liu, G. Li, A. Navrotsky, J.B. Goates, B.F. Woodfield, Heat capacities and thermodynamic functions of TiO_2 anatase and rutile: analysis of phase stability, Am. Mineral, 94 (2009) 236-243.

[44] W.P. Jones, B.E. Launder, The prediction of laminarization with a two-equation model of turbulence, International Journal of Heat and Mass Transfer, 15 (1972) 301-314.

[45] W.P. Jones, B.E. Launder, The calculation of low-Reynolds-number phenomena with a two-equation model of turbulence, International Journal of Heat and Mass Transfer, 16 (1973) 1119-1130.

[46] Y.G. Lai, R.M.C. So, On near-wall turbulent flow modelling, Journal of Fluid Mechanics, 221 (1990) 641-673.

[47] H.K. Myong, N. Kasagi, A new approach to the improvement of k-ϵ turbulence model for wall-bounded shear flows, International Journal of JSME, 33 (1990) 63-72.

[48] H. Blasius, Grenzschichten in Flussigkeiten mit kleiner reibung (German), Z. Math. Physics 56 (1908) 1-37.

[49] B.S. Petukhov, Heat transfer and friction in turbulent pipe flow with variable physical properties, New York, 1970.

[50] R.H. Notter, M.W. Rouse, A solution to the Graetz problem-III. Fully developed region heat transfer rates, Chemical Engineering Science, 27 (1972) 2073-2093.

[51] V. Gnielinski, New equations for heat and mass transfer in turbulent pipe and channel flow, International Chemical Engineering, 16 (1976) 359-368.

[52] B.C. Pak, Y.I. Cho, Hydrodynamic and heat transfer study of dispersed fluids with submicron metallic oxide particles, Experimental Heat Transfer, 11 (1998) 151-170.

[53] S. Lee, S.U.S. Choi, S. Li, J.A. Eastman, Measuring thermal conductivity of fluids containing oxide nanoparticles, Journal of Heat Transfer, 121 (1999) 280-289.

[54] X. Wang, X. Xu, S.U.S. Choi, Thermal conductivity of liquid with suspension of nanoparticles-fluid mixture, Journal of Thermophysics and Heat Transfer, 13 (1999) 474-480.

[55] A. Einstein, Investigating on the theory of Brownian motion, New York, 1956.

[56] H.C. Brinkman, The viscosity of concentrated suspensions and solution, Journal of Chemical Physics, 20 (1952) 571-581.

[57] S.E.B. Maiga, C.T. Nguyen, N. Galanis, G. Roy, T. Mare, M. Coqueux, Heat transfer enhancement in forced convection laminar tube flow by using nanofluids, in: CHT-04 International Symposium Advances Computational heat Transfer, Norway, 2004, pp. 25.

[58] R.L. Hamilton, O.K. Crosser, Thermal conductivity of heterogeneous two-component systems, I and EC Fundamentals 1(1962) 187-191.

[59] S.K. Das, S.U.S. Choi, W. Yu, T. Pradeep, Nanofluids science and technology, John Wiley and Sons, 2008.

[60] S. Suresh, M. Chandrasekar, S.C. Sekhar, Experimental studies on heat transfer and friction factor characteristics of CuO/water nanofluid under turbulent flow in a helically dimpled tube, Experimental Thermal and Fluid Science 35 (2011) 542-549.

[61] R. Mosurkal, L.A. Samuelson, K.D. Smith, P.R. Westmoreland, V.S. Parmar, F. Yan, Nanocomposites of TiO_2 and siloxane copolymers as environmentally safe flame retardant materials, Journal of Macromolecular Science Part A Pure and Applied Chemistry, 45 (2008) 924–946.

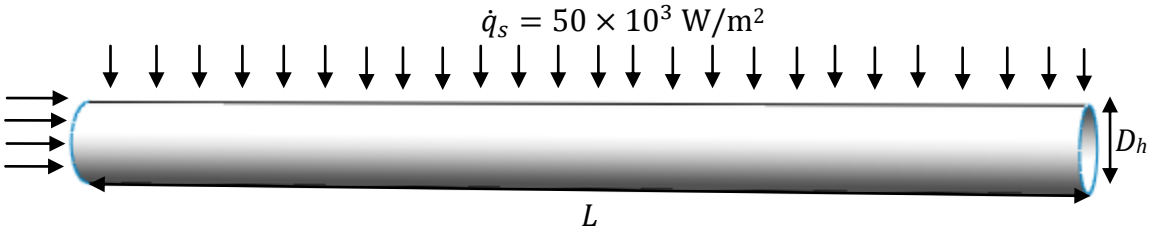

Figure 1: Schematic diagram of the geometry under consideration

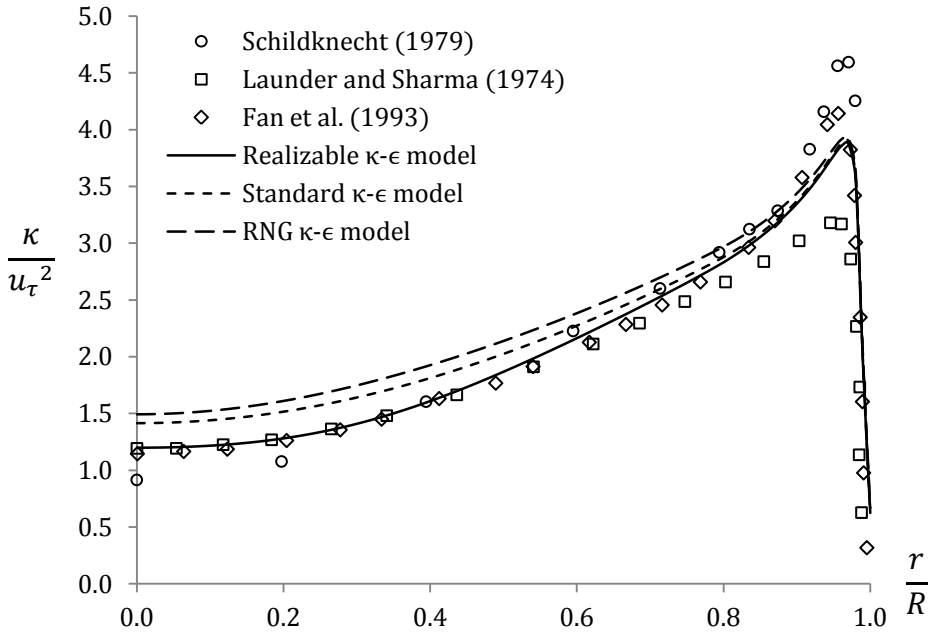

Figure 2: Variation of radial turbulent kinetic energy at the fully developed location near the outlet using different κ - ϵ models for Re = 21800

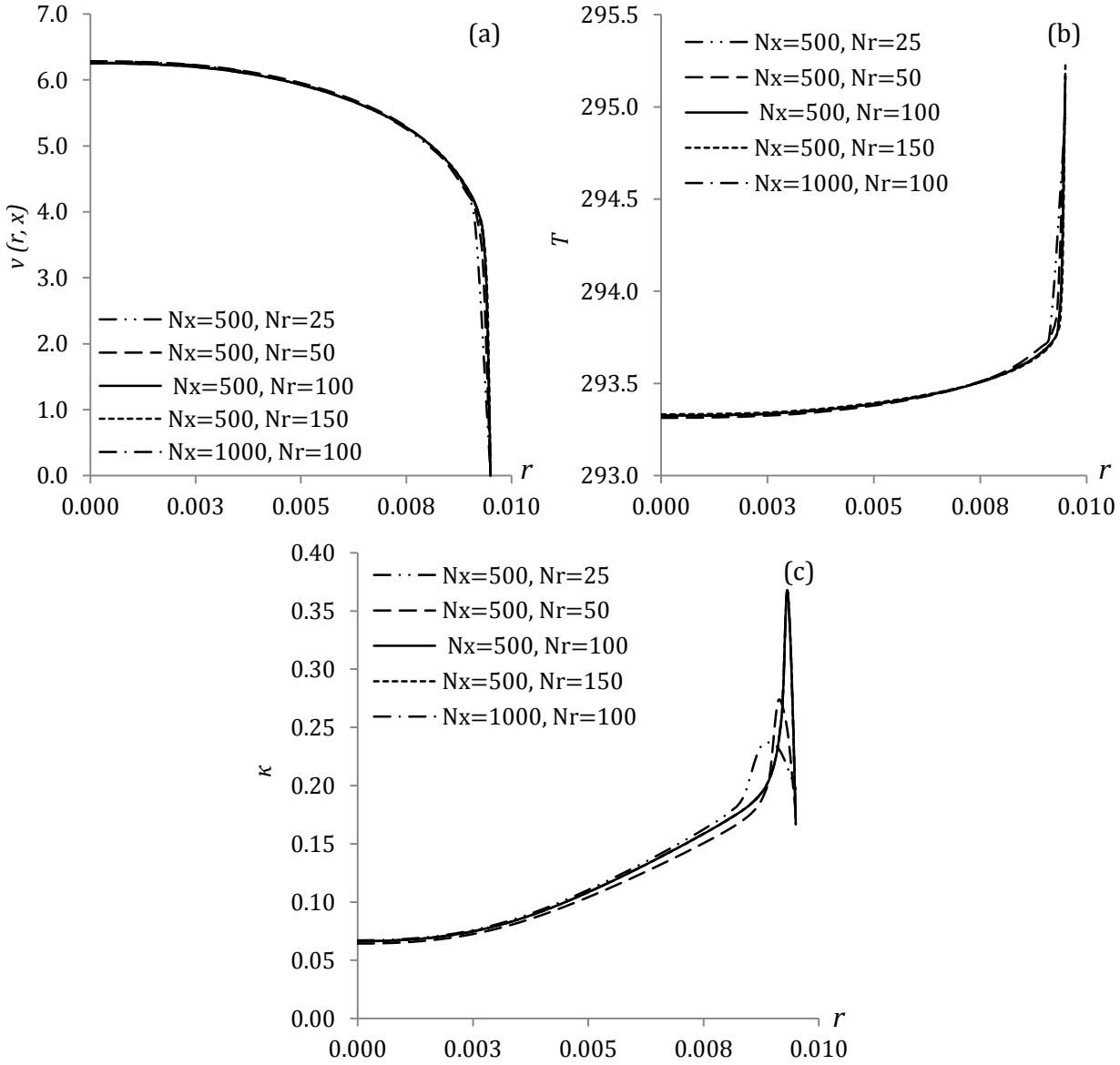

Figure 3: Variation of radial (a) velocity, (b) temperature and (c) turbulent kinetic energy at the fully developed location near the outlet

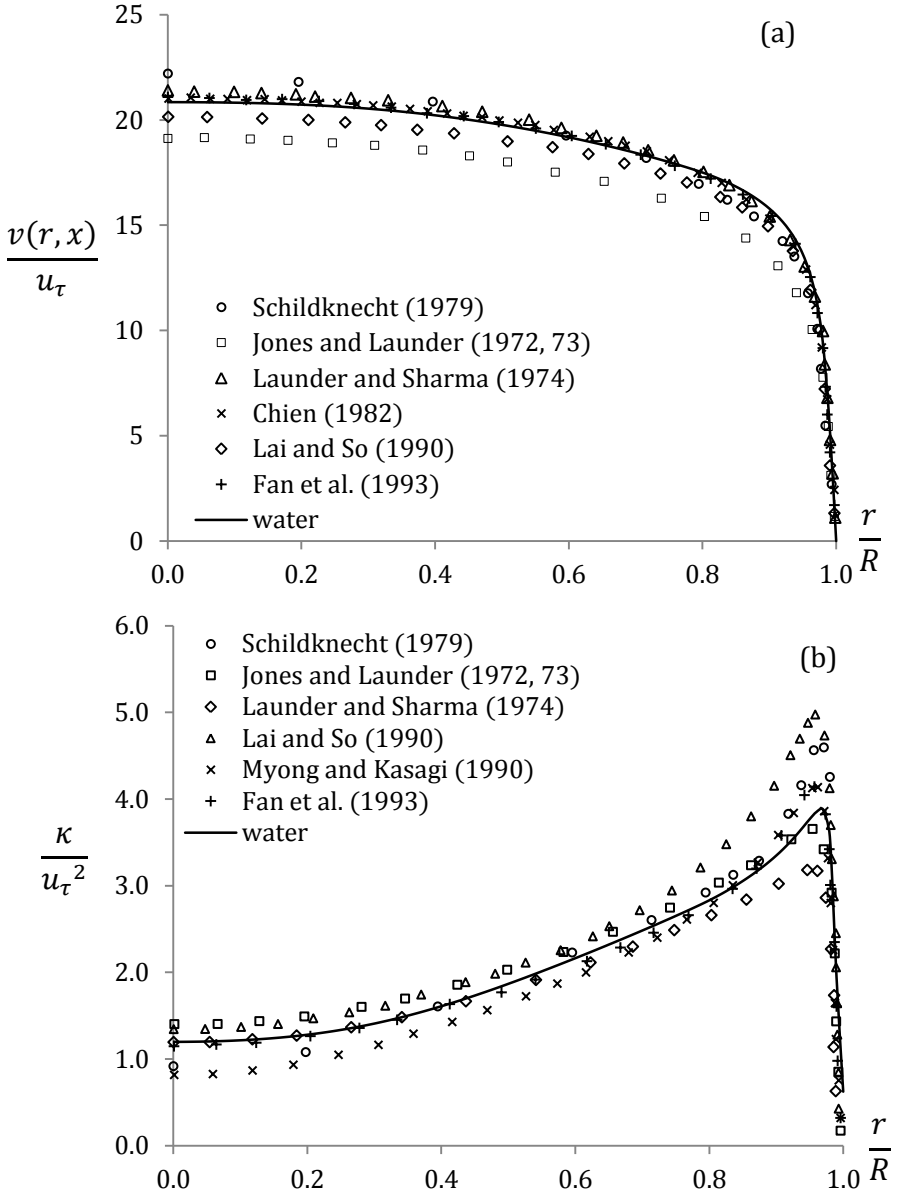

Figure 4: Variation of radial (a) velocity and (b) turbulent kinetic energy at the fully developed location near the outlet for *Re* = 21800 and *Pr* = 7.04.

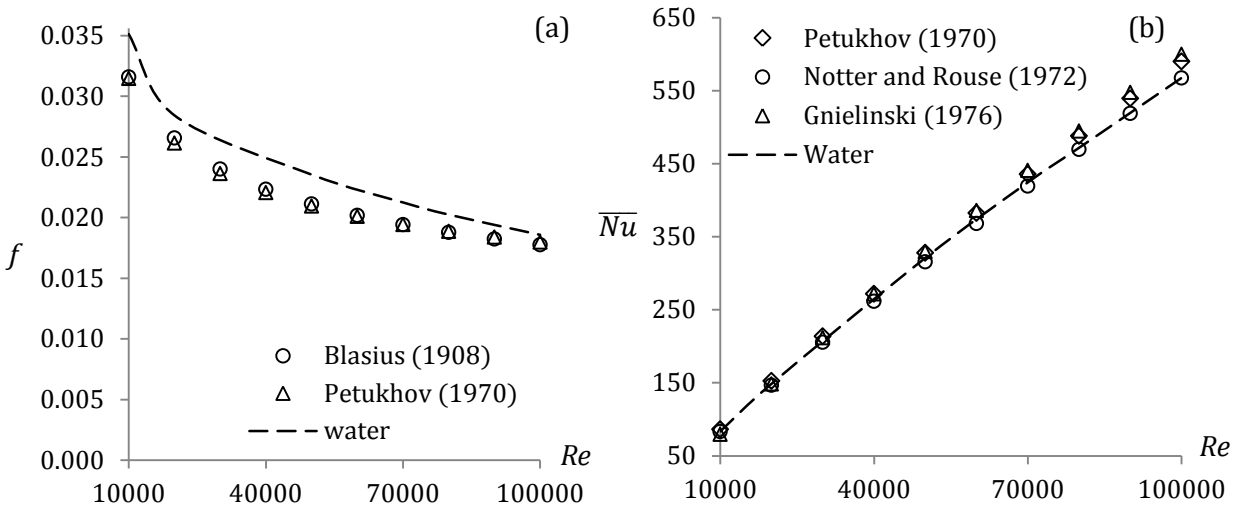

Figure 5: Comparison of the (a) Darcy friction factor, f and (b) average Nusselt number, $\overline{Nu}$ with the different correlations for different Re

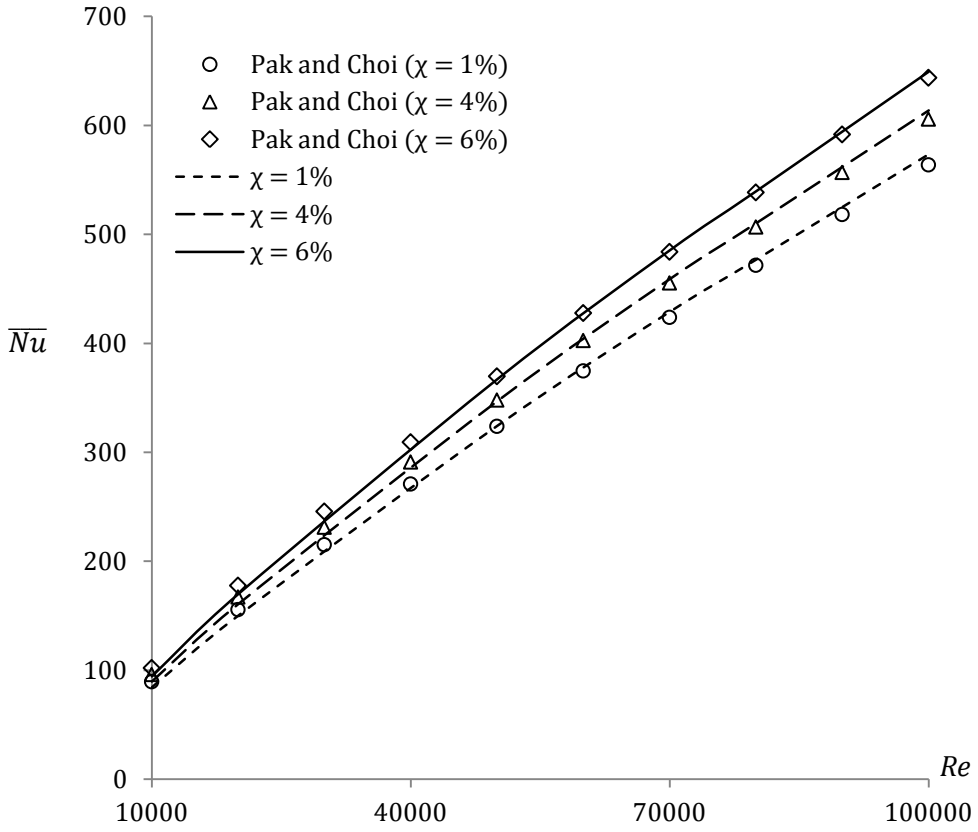

Figure 6: Comparison of the average Nusselt number for Al_2O_3-H_2O nanofluid with the Pak and Cho [52] correlation for different *Re*

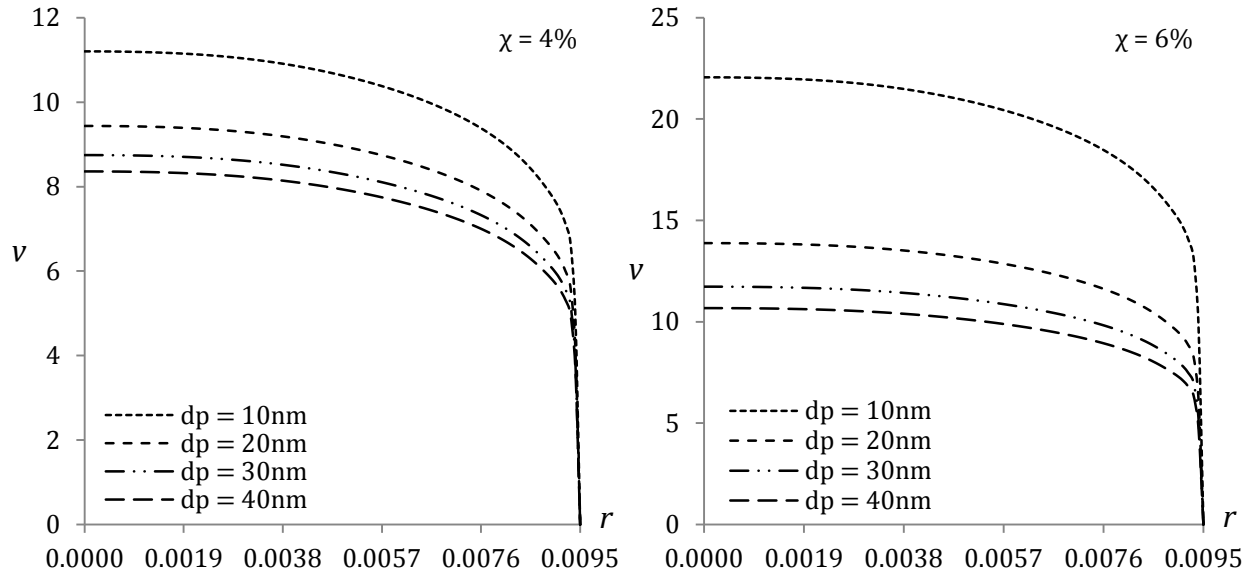

Figure 7: Variation of fully developed radial velocity profile for Al_2O_3-water nanofluids, nanoparticle volume concentration of 4% and 6%, $Re = 100 \times 10^3$ and nanoparticles size diameter of 10, 20, 30 and 40 *nm*

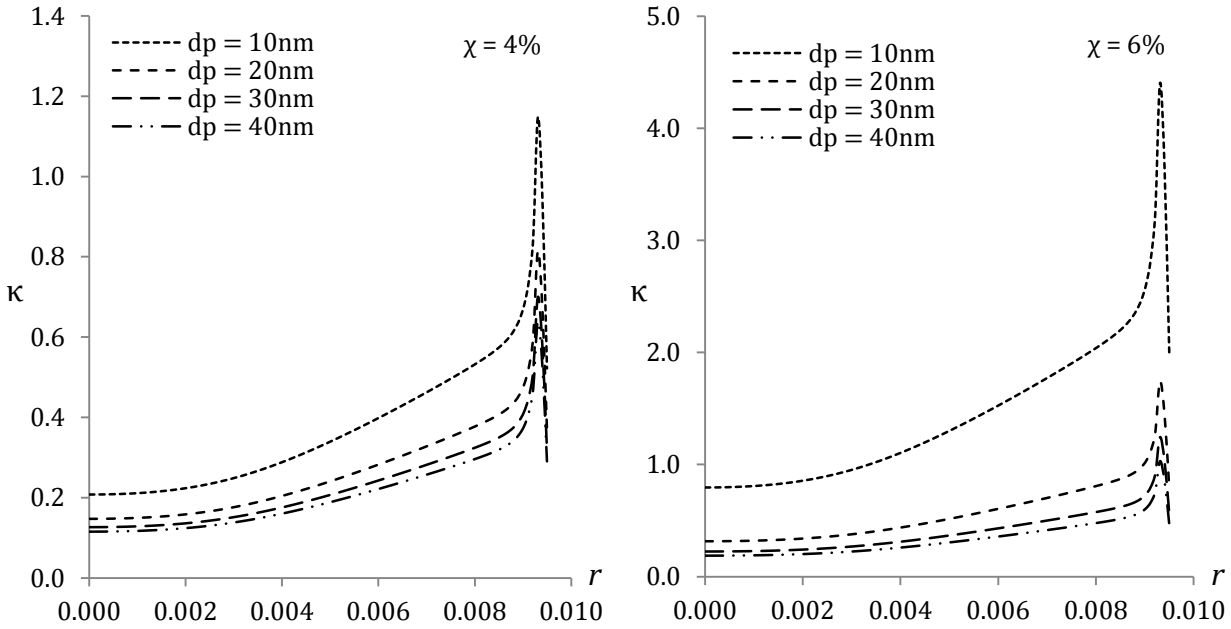

Figure 8: Variation of radial turbulent kinetic energy for Al_2O_3-water nanofluids, nanoparticle volume concentration of 4% and 6%, $Re = 100 \times 10^3$ and nanoparticles size diameter of 10, 20, 30 and 40 *nm*

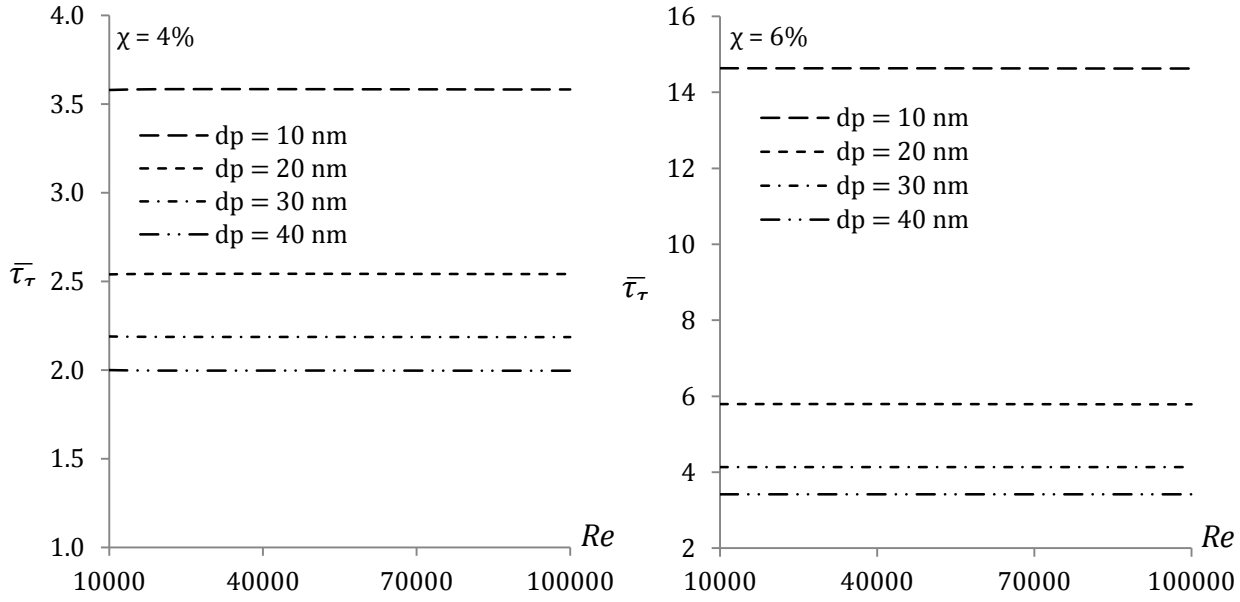

(a) Al_2O_3-H_2O nanofluid

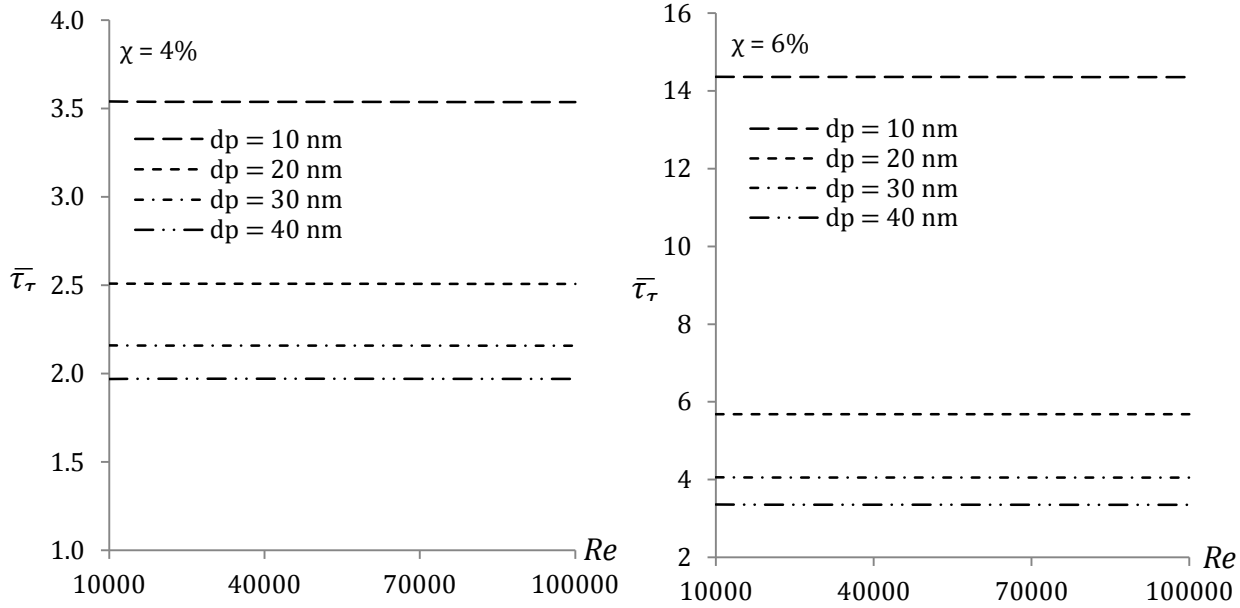

(b) TiO_2-H_2O nanofluid

Figure 9: Variation of average shear stress ratio with Reynolds number for Al_2O_3-water and TiO_2-water nanofluids, nanoparticle volume concentration of 4% and 6% and nanoparticles size diameter of 10, 20, 30 and 40 *nm*

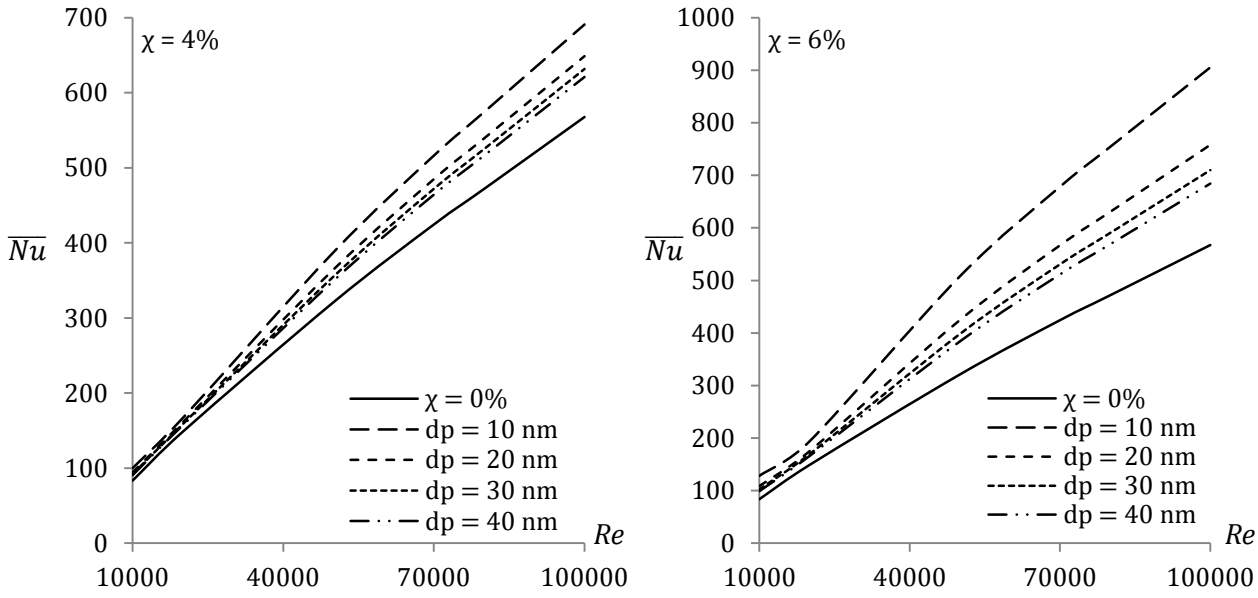

(a) Al_2O_3-H_2O nanofluid

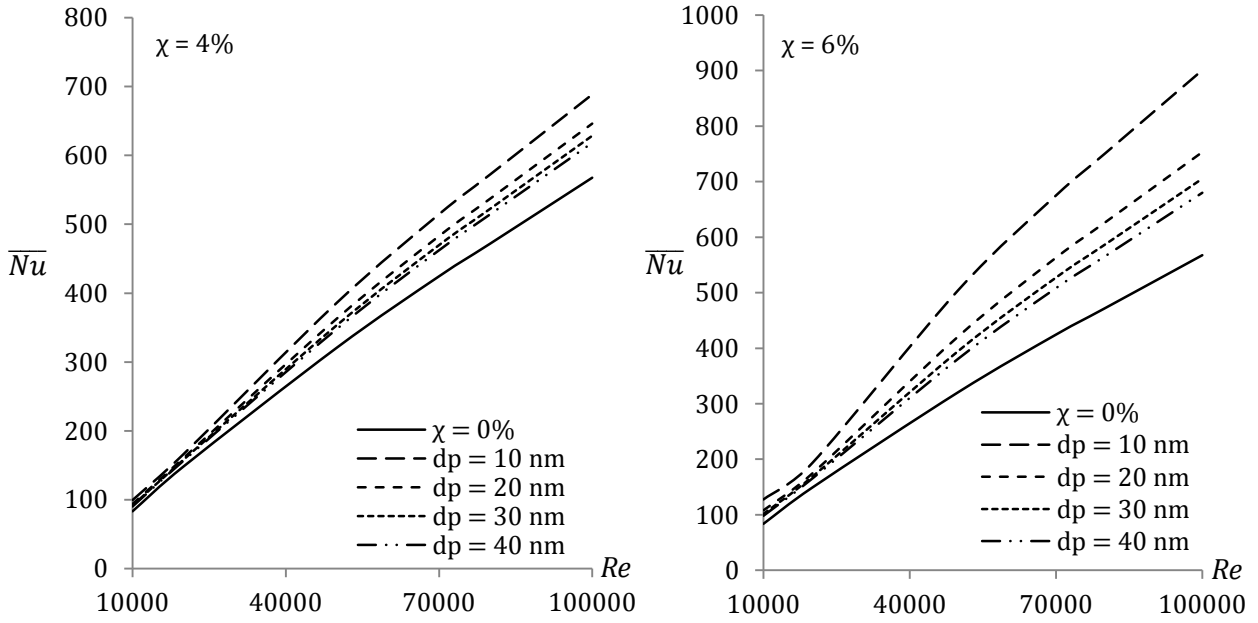

(b) TiO_2-H_2O nanofluid

Figure 10: Variation of average Nusselt number with Reynolds number for Al_2O_3-water and TiO_2-water nanofluids, nanoparticles volume concentration of 4% and 6% and nanoparticles size diameter of 10, 20, 30 and 40 *nm*

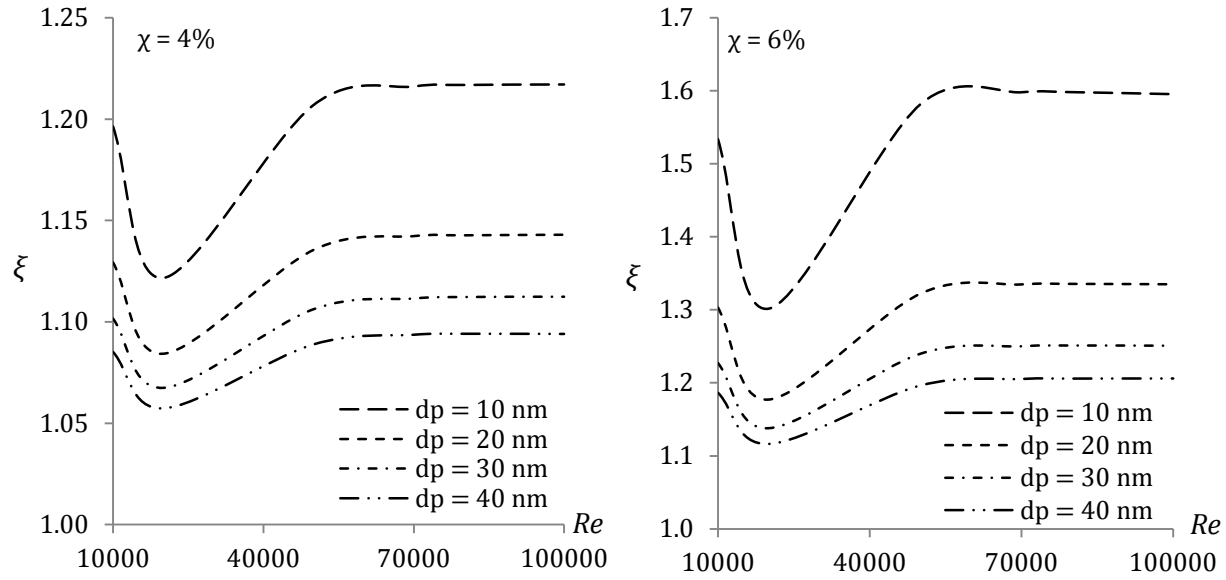

(a) Al_2O_3-H_2O nanofluid

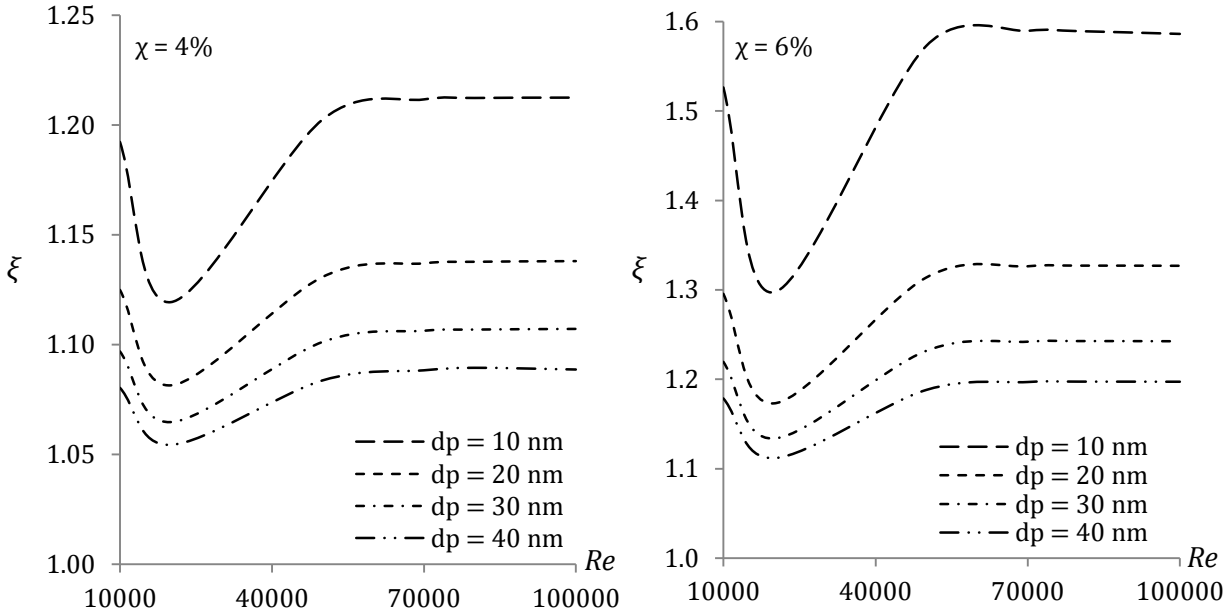

(b) TiO_2-H_2O nanofluid

Figure 11: Variation of thermal performance factor with Reynolds number for Al_2O_3-water and TiO_2-water nanofluids, nanoparticles volume concentration of 4% and 6% and nanoparticles size diameter of 10, 20, 30 and 40 *nm*

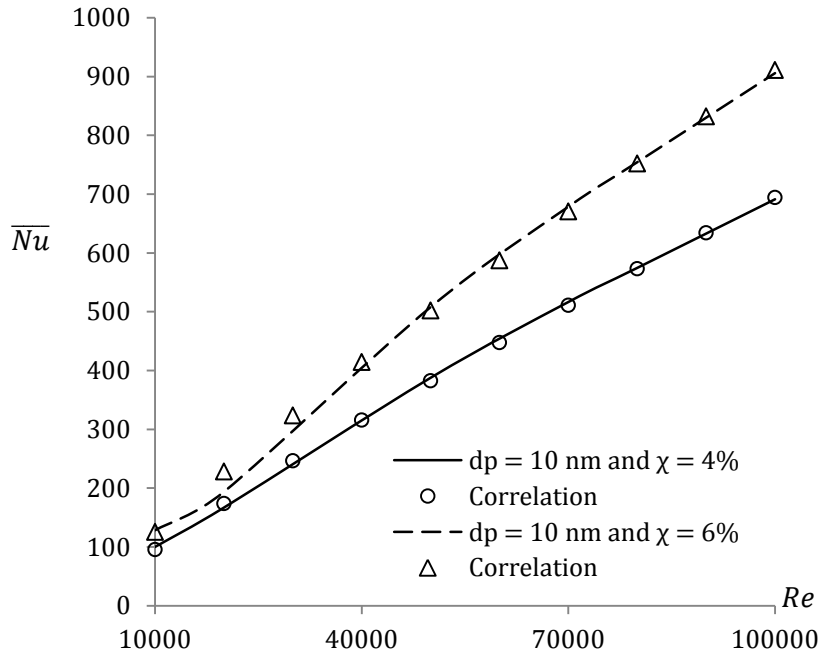

Al_2O_3-H_2O nanofluid

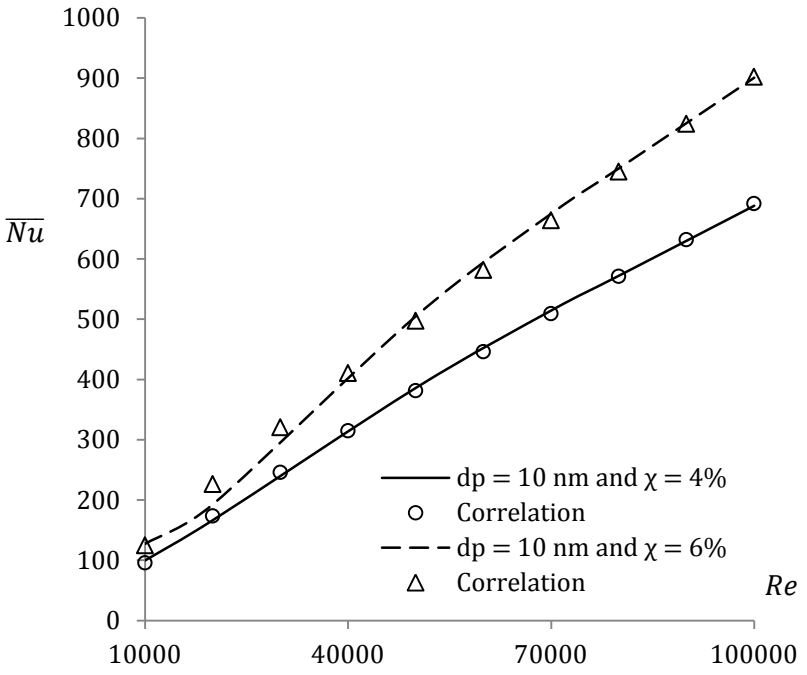

TiO_2-H_2O nanofluid

Figure 12: Comparisons of the proposed correlations with the numerical results for Al_2O_3-water and TiO_2-water nanofluids